JOURNAL OF Materials CHEMISTRY

$LaSrMn_{0.5}Ni_{0.5}O_{4+\delta}$: spin and oxidation state in the K_2NiF_4 structure

J. E. Millburn and M. J. Rosseinsky*

Inorganic Chemistry Laboratory, Department of Chemistry, University of Oxford, South Parks Road, Oxford, UK OX1 3QR

Magnetic and structural data on the K_2NiF_4 structure oxide $LaSrMn_{0.5}Ni_{0.5}O_{4+\delta}$ are reported. Powder X-ray and electron diffraction show that the samples adopt the tetragonal *I*4/*mmm* space group without cation ordering. The absence of cation ordering together with structural considerations and magnetic data indicate that both cations are in the +III oxidation state, with high spin Ni^{III} in contrast to both the three-dimensional perovskite $LaMn_{0.5}Ni_{0.5}O_3$ and the K_2NiF_4 phase $LaSrCr_{0.5}Ni_{0.5}O_4$. The spin and oxidation state distributions account for the suppression of the antiferromagnetic long-range order of $LaSrMnO_4$ and the observation of hysteresis characteristic of spin- or cluster glass behaviour below 90 K. The irreversible magnetism, but not that in the high-temperature Curie–Weiss region, is slightly altered by annealing single phase samples. The higher divergence temperature in the annealed sample is consistent with greater homogeneity of the cation distribution, as found for canonical RKKY spin glasses.

Introduction

Transition metal oxides with the K_2NiF_4 and related structures have been widely studied in recent years in the areas of superconductivity and catalysis, while the charge and related 'stripe' ordering in $La_{2-x}Sr_xNiO_4$ for $x=0.33$–0.5[1,2] has been the subject of fundamental interest. The ordering of Mn^{III} and Mn^{IV} valences has recently been studied in detail, in the context of colossal magnetoresistance, in $La_{0.5}Ca_{0.5}MnO_3$[3] and $La_{0.5}Sr_{1.5}MnO_4$.[4] The subtlety of the interactions controlling such transitions is shown by the suppression of this 'charge ordering' in $Nd_{0.5}Sr_{1.5}MnO_4$, where the Jahn–Teller distortion of the MnO_6 unit is more pronounced.[5] Substitution of other transition metal cations on the B site can produce physical phenomena related to those displayed above and has been widely investigated in the perovskite structure, *e.g.* the ferromagnetism of $La_{1-x}Sr_xMnO_3$ is retained in $LaCr_{1-x}Mn_xO_3$[6] where the d^3–d^4 ferromagnetic exchange in the insulator plays the role of double exchange in the metallic pure manganate, while spin and cluster glass together with inhomogeneous ferromagnetic behaviour has recently been demonstrated for $LnMn_{1-x}Co_xO_3$ phases.[7] A detailed investigation of site-diluted Fe perovskites using Mössbauer spectroscopy shows that competition between nearest- and next-nearest-neighbour exchange interactions can be important in producing unusual magnetic relaxation.[8] Such B site co-substitutions can also produce interesting chemical behaviour: reduction of $LaCr_{0.6}Ni_{0.4}O_3$ results in the Cr^{III}/Ni^{II} oxide $LaSrCr_{0.6}Ni_{0.4}O_{2.8}$,[9] of interest in the context of fuel-cell applications. The perovskite is well known to be the $n=\infty$ member of the $A_{n+1}B_nO_{3n+1}$ Ruddlesden–Popper series, but, aside from some early pioneering work[10–13] there have been fewer studies of such B site cosubstitution in the $n=1$ homologue, K_2NiF_4 structure. The $LaSrNi_{1-x}Cr_xO_4$ phases are canonical spin-glasses[14] whose magnetism suggests an interpretation of the complex low-temperature magnetic behaviour of $La_{2-x}Sr_xNiO_4$.[15] The reduction of $LaSrCr_{0.5}Ni_{0.5}O_4$ produces $La_2Sr_2CrNiO_7$, a Ni^{I} oxide with an unprecedented thermal stability.[14]

Before this physical and chemical behaviour can be understood, there are complex issues of oxidation state identification in these mixed B cation systems. An example of this is the substitution of manganese into metallic $LaNiO_3$.[16–24] $LaMn_{0.5}Ni_{0.5}O_3$ is a three-dimensional ferromagnet ($T_c=$ 270–300 K; $m_{sat}=2.5\ \mu_B$) but the oxidation state distribution has long been a matter of controversy. The observation of X-ray superlattice reflections and ^{55}Mn NMR measurements have led some workers to claim that Mn^{IV} and Ni^{II} are present,[16,18,25] while X-ray photoelectron and absorption spectroscopies have been used to indicate the presence of Mn^{III} and low spin Ni^{III}.[21,23,24] Both the saturation moment of the ferromagnet and the Curie law moments turn out to be insensitive to these different oxidation state distributions. A detailed magnetic study of $LaMn_{1-x}Ni_xO_3$ indicates that while the $x=0.5$ composition is a true three-dimensional ferromagnet, phases with $x<0.2$ are spin glasses.[24] In this paper, we contrast this well studied $n=\infty$ Mn/Ni member of the $A_{n+1}B_nO_{3n+1}$ Ruddlesden–Popper series with the $n=1$ analogue $LaSrMn_{0.5}Ni_{0.5}O_4$, using low field magnetisation and structural probes, including comparison with the low-spin Ni^{III} phases $LaSrCr_{0.5}Ni_{0.5}O_4$ and $La_{0.9}Nd_{0.1}SrCr_{0.5}Ni_{0.5}O_4$. The latter phase is studied to indicate whether the extent of Jahn–Teller distortion at low-spin Ni^{III} is sensitive to A cation size and electronegativity, given the influence demonstrated in $Ln_{0.5}Sr_{1.5}MnO_4$.[5] The results add a new complication to spin and oxidation state identification in mixed B site Ruddlesden–Popper phases, as they clearly indicate that a change of co-substituent on the B site changes the Ni^{III} spin state from low spin in $LaSrCr_{0.5}Ni_{0.5}O_4$ to high spin in $LaSrMn_{0.5}Ni_{0.5}O_4$.

Experimental

Stoichiometric quantities of La_2O_3 (99.999%, Aldrich), predried in air at 800 °C to remove adsorbed water and CO_2, $SrCO_3$ (99.994%, Alfa), Ni powder (99.999%, Aldrich) and Mn flake (99.99%, Aldrich) were dissolved in 150 ml of a 1:1 solution of Analar 6 M nitric acid and distilled water. Analar ethylene glycol (5 ml, 99.5%, BDH) and one equivalent of citric acid per mole of M^{3+} cation (99.5%, BDH) were added and the solution heated at 150 °C on a hot plate with constant stirring for approximately 3 h. Initial decomposition of the gel at 350 °C for 24 h followed by heating at 800 °C for between 24 and 48 h was followed by pressing into 13 mm pellets. As previously found in the $LaSrCr_{1-x}Ni_xO_4$ series, the preparation of phase-pure samples required close attention to the synthesis atmosphere. Reaction in oxygen or air at 1200 °C lead to the formation of $n=\infty$ perovskite, only apparent in low field magnetisation measurements and upon close inspection of Rietveld refinements. Successful preparation of $LaSrMn_{0.5}Ni_{0.5}O_4$ free of this impurity requires the exclusion

Table 1 Summary of the synthesis conditions for sample **B** of $LaSrMn_{0.5}Ni_{0.5}O_4$. Sample **C** was produced from sample **B** as discussed in the text.

temperature/°C (atmosphere)	time/hours
350 (air)	8
800 (air)	72
900 (air)	67
1200 (Ar)	120

of O_2, using reaction under flowing dried, deoxygenated argon at the temperatures described in Table 1, with regular regrinding and pelletising. Once the purity of this sample (**B**) had been confirmed, both magnetically and by successful single phase refinement of powder X–ray diffraction data, the sample was split into two 1 g parts and one half was subsequently annealed at the higher temperature of 1300 °C for 78 h under Ar to yield sample **C**, in order to explore the effect of further annealing on the physical properties. The progress of the reactions were monitored by powder X-ray diffraction (Cu-Kα radiation) using a Philips automated PW 1710 diffractometer.

Powder X-ray diffraction data for structural refinement were collected in Bragg–Brentano geometry on a Siemens D5000 diffractometer (Cu-Kα_1 radiation), the samples being mounted on a silicon wafer, over the range $15 \leqslant 2\theta/^\circ \leqslant 120$, $\Delta 2\theta = 0.02^\circ$. Rietveld refinement[26] was performed using the GSAS [27] program suite. The refinements employed a 10 term shifted Chebyshev polynomial background function and 3 term pseudo-Voigt peak shape function.

The interpretation of the behaviour of $LaSrMn_{0.5}Ni_{0.5}O_4$ requires comparison with the structure of $LaSrCr_{0.5}Ni_{0.5}O_4$, which was reported previously but only characterised by X-ray powder diffraction.[14] Room temperature powder neutron diffraction data were collected on 5 g samples contained in cylindrical vanadium cans. $La_{0.9}Nd_{0.1}SrCr_{0.5}Ni_{0.5}O_4$ was measured on the high intensity, medium resolution Polaris time-of-flight (TOF) diffractometer at the ISIS spallation source at the Rutherford Appleton Laboratories. For this compound data from the A (0.5–8.15 Å), C (0.2–3.2 Å) and E (0.3–4.1 Å) detector banks were refined simultaneously by the Rietveld method within the GSAS program suite, using a 3 term pseudo-Voigt function convoluted with two back-to-back exponentials to model the peak shape and a 12 term cosine Fourier series background expression for each of the three banks. High resolution powder neutron diffraction data were collected for $LaSrCr_{0.5}Ni_{0.5}O_4$ at room temperature on the HRPD TOF diffractometer, also at ISIS. Measurements were taken at the 1 m sample position over the TOF range 30 000–130 000 μs corresponding to a d-spacing range of 0.6–2.6 Å with a $\Delta d/d$ resolution of 5×10^{-4}. A 10 term shifted Chebyshev background function and a 3 term pseudo-Voigt peak shape function were used in the Rietveld refinement of the data. The raw data in both cases were normalised to the incident beam and calibrated for detector efficiency by dividing by a standard vanadium run collected under the same conditions prior to refinement.

Magnetic data for samples **B** and **C** were collected over the temperature range $5 \leqslant T/\mathrm{K} \leqslant 300$ in a 0.01 T field using a Quantum Design MPMS SQUID magnetometer. Field cooled hysteresis $M(H)$ measurements were also carried out on sample **B** at a number of temperatures. For the 3 T loops, 0.2 T field steps were employed for $1 \leqslant B/\mathrm{T} \leqslant 3$ and 0.1 T steps for $-1 \leqslant B/\mathrm{T} \leqslant 1$ while for the 0.2 T loop 0.005 T steps were used.

Thermogravimetric analysis was carried out using a Rheometric Scientific STA 1500 thermal analyser. Samples weighing approximately 50 mg contained in platinum crucibles were placed in the apparatus which was then purged for at least 30 min with H_2, predried over activated molecular sieves. Samples were subsequently heated to 950 °C at a rate of 5 °C min^{-1} under the gas flow and held at this temperature for up to 3 h before being allowed to cool, under the gas flow, to room temperature at the cooling rate of the furnace.

The Ni^{III} content of the samples was determined by iodometric titration against a standardised potassium thiosulfate solution, the titrations being repeated several times to ensure accurate and consistent results.[28] The thiosulfate solution was standardised against the primary standard potassium iodate.[29]

High resolution transmission electron microscopy (HRTEM) measurements were made on sample **C**. The specimen was ultrasonically dispersed in Analar chloroform before being transferred to a lacey carbon-coated copper grid (Agar, 200 mesh). Data were collected using a JEOL 4000EX electron microscope operated at 400 kV (point resolution = 1.6 Å). All high resolution images were recorded at, or close to, optimum Scherzer defocus conditions.

Results

Oxygen content analysis and thermogravimetric analysis

The oxygen concentrations per formula unit for samples B and C were 4.01(2) and 4.00(2) respectively. It proved impossible to confirm the oxygen contents established from the iodometry by means of thermogravimetric analysis. Even when the samples were heated to 950 °C and held at this temperature for up to 3 h under the H_2 flow, the reduction did not proceed to completion. No clear plateaux were visible in the weight loss for either sample **B** or **C**, although there are several inflection points in the curves. A typical weight loss curve for sample **C**, heated to 900 °C at 5 °C min^{-1} under H_2 and then held at this temperature for 2 h, is shown in Fig. 1. Inspection of the X-ray powder diffraction pattern of the sample after this treatment reveals the presence of La_2O_3, SrO, Ni metal, Mn_2O_3 and MnO in addition to a residual K_2NiF_4 phase [a = 3.813(1) Å, c = 13.070(7) Å].

X-Ray powder diffraction

Rietveld analysis of the X-ray powder diffraction patterns of samples prepared under flowing O_2 indicated a small quantity of $n = \infty$ perovskite, whose phase fraction increased with both annealing time and temperature. The structural parameters from the K_2NiF_4 phase were, however, consistent with those found in phase-pure samples.

Refinement of the data for pure samples prepared under argon indicated that the space group was $I4/mmm$. Refinement required the use of a correction for preferred orientation along the [001] direction. For sample **C**, separate isotropic temperature factors could be refined for the metal atom A and B sites, while oxygen temperature factors were fixed at 0.01 $\mathrm{Å}^2$. The

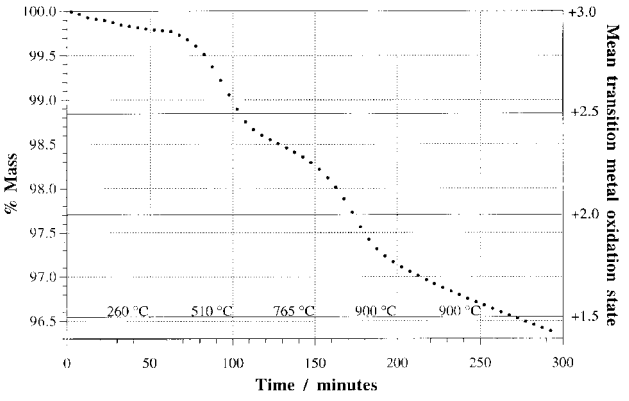

Fig. 1 Thermogravimetric analysis (TGA), under a flowing pure hydrogen atmosphere, of $LaSrMn_{0.5}Ni_{0.5}O_4$ (sample **C**). The first 200 min of the experiment involve ramping the temperature to 900 °C, followed by a 100 min hold at this temperature.

Table 2 Structural parameters derived from the Rietveld refinement of powder X-ray diffraction data for $LaSrMn_{0.5}Ni_{0.5}O_4$, samples **B** and **C**

$LaSrMn_{0.5}Ni_{0.5}O_4$		**B**	**C**
a/Å		3.83892(7)	3.83887(4)
c/Å		12.5643(2)	12.5955(1)
V/Å^3		185.165(6)	185.618(5)
La/Sr	z	0.35947(6)	0.36003(9)
	U_{iso}/Å^2	0.004[a]	0.0029(3)
Mn/Ni	U_{iso}/Å^2	0.004[a]	0.0068(9)
O(1)	z	0.1669(4)	0.1635(6)
	U_{iso}/Å^2	0.01[a]	0.01[a]
O(2)	U_{iso}/Å^2	0.01[a]	0.01[a]
R_{wp}(%)		7.9	9.9
R_p(%)		6.2	7.8
RF^2(%)		5.8	9.9
R_F(%)		3.2	6.1
χ^2		1.3	1.5

[a]Thermal parameters were fixed as described in the text. The atoms were refined in the following Wyckoff positions of space group no. 139, *I*4/*mmm*: 4 La/Sr and 4O(1) in (e) (4*mm*) (0, 0, *z*); 2 Ni/Mn in (a) (4/*mmm*) (0, 0, 0); 4 O(2) in (c) (*mmm*) (0, 1/2, 0).

metal site occupancies were not refined. The positional, thermal and agreement parameters are given in Table 2 for the refinement shown in Fig. 2. The relevant bond lengths derived from this analysis are shown in Table 5, (see later).

Neutron powder diffraction

The crystal structures of $La_{0.9}Nd_{0.1}SrCr_{0.5}Ni_{0.5}O_4$ and $LaSrCr_{0.5}Ni_{0.5}O_4$ were refined from room temperature powder neutron diffraction data in the *I*4/*mmm* tetragonal space group.

For the former sample, the inclusion of an absorption correction in the final refinement was necessary to obtain a satisfactory fit to the intensities at longer *d*-spacings. The positional and thermal parameters obtained from the combined refinement of the data from each of the three detector banks are given in Table 3, and the observed, calculated and difference profiles are shown in Fig. 3(a). For $LaSrCr_{0.5}Ni_{0.5}O_4$, the presence of several small impurity peaks in the diffraction pattern led to the inclusion of NiO as a minority phase [1.41(7)% mole fraction] in the final refinement. The positional and thermal parameters for $LaSrCr_{0.5}Ni_{0.5}O_4$ are given in Table 3, and the observed, calculated and difference profiles are shown in Fig. 3(b). In both cases, refinement of oxygen occupancies confirms that the oxygen stoichiometry is 4.00 within experimental error. Anisotropic displacement parameters were successfully refined for all atoms in the unit cell in both cases and the resulting ellipsoids for $LaSrCr_{0.5}Ni_{0.5}O_4$ are shown in Fig. 4. The refined ellipsoids are similar for equivalent atoms in both samples. Refinement of the relative nickel/chromium content, with the overall transition metal site

Table 3 Structural parameters obtained from the room temperature Rietveld refinement of powder neutron diffraction data for $La_{0.9}Nd_{0.1}SrCr_{0.5}Ni_{0.5}O_4$ and $LaSrCr_{0.5}Ni_{0.5}O_4$

		$La_{0.9}Nd_{0.1}SrCr_{0.5}Ni_{0.5}O_4$	$LaSrCr_{0.5}Ni_{0.5}O_4$
a/Å		3.82287(3)	3.82756(1)
c/Å		12.6201(1)	12.63939(6)
V/Å^3		184.434(2)	185.170(1)
mole fraction (%)		—	98.59(7)
La/Sr/Nd	z	0.35893(3)	0.35911(9)
	U_{11}/Å^2	0.00720(9)	0.0071(4)
	U_{33}/Å^2	0.0053(1)	0.0073(5)
Cr/Ni	U_{11}/Å^2	0.0038(1)	0.0043(5)
	U_{33}/Å^2	0.0079(2)	0.0108(8)
	occupancy	Ni 0.499(2)	Ni 0.515(8)
		Cr 0.501(2)	Cr 0.485(8)
O(1)	z	0.16669(4)	0.1669(1)
	U_{11}/Å^2	0.0159(1)	0.0165(6)
	U_{33}/Å^2	0.0130(2)	0.0113(8)
	occupancy	1.011(2)	1.011(8)
O(2)	U_{11}/Å^2	0.0081(1)	0.0083(7)
	U_{22}/Å^2	0.0063(1)	0.0082(7)
	U_{33}/Å^2	0.0110(2)	0.0105(9)
	occupancy	0.999(2)	0.989(9)
R_{wp}(%)		2.2	7.5
R_p(%)		3.3	6.0
RF^2(%)		A = 3.4	12.5
		C = 3.6	
		E = 3.1	
R_F(%)		A = 2.6	3.7
		C = 2.5	
		E = 1.9	
χ^2		4.7	6.3

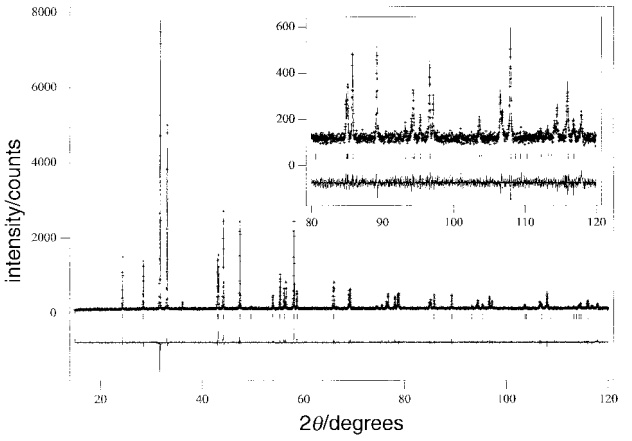

Fig. 2 Observed (markers), calculated (line) and difference profiles for the X-ray Rietveld refinement of $LaSrMn_{0.5}Ni_{0.5}O_4$ (sample **C**) in the *I*4/*mmm* space group. The inset shows an enlargement of the fit over the range $80 \leqslant 2\theta/^\circ \leqslant 120$. Tick marks indicate the location of Bragg peaks.

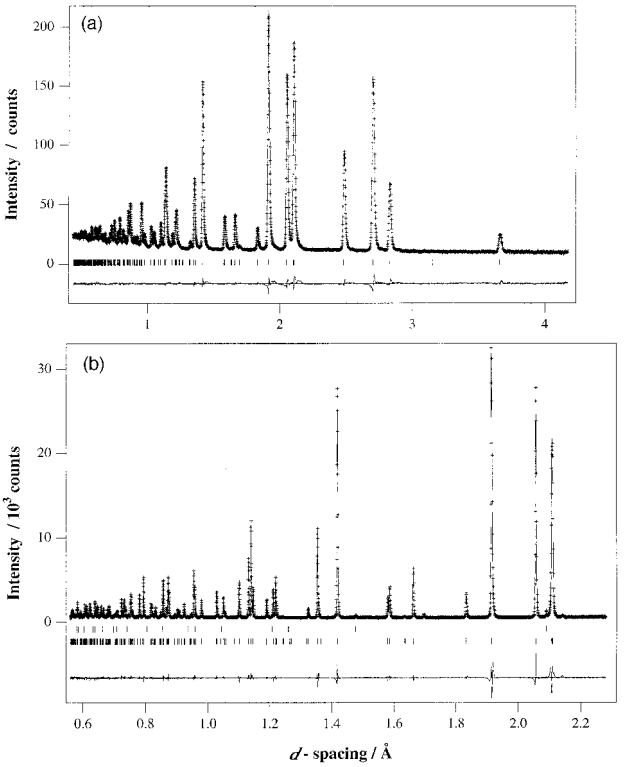

Fig. 3 Rietveld refinements (presented as in Fig. 2) of the room temperature TOF powder neutron data of (a) $La_{0.9}Nd_{0.1}SrCr_{0.5}Ni_{0.5}O_4$ (POLARIS E bank) and (b) $LaSrCr_{0.5}Ni_{0.5}O_4$ (HRPD) in the *I*4/*mmm* space group (the upper set of tick marks correspond to NiO impurity)

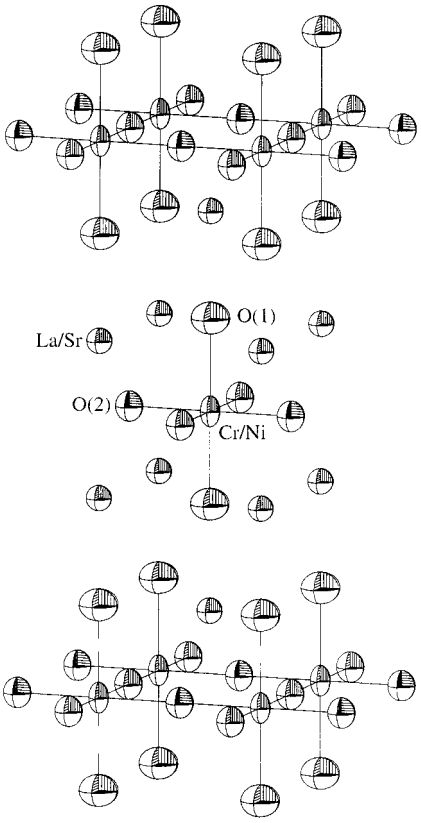

Fig. 4 ORTEP representation of the structure of $LaSrCr_{0.5}Ni_{0.5}O_4$. The atoms are represented as 90% thermal ellipsoids.

occupancy being constrained to 1.0, also confirms the 1:1 ratio within error. Attempts to refine the data in lower symmetry tetragonal and orthorhombic space groups proved unstable. It is important to note that the scattering length contrast and measured *d*-spacing range are such that Cr/Ni ordering would have been easily detectable in the current experiments.

Comparison with the results of X-ray powder diffraction refinements on the same $LaSrCr_{0.5}Ni_{0.5}O_4$ sample indicate that the accuracy with which X-ray powder diffraction determines the B—O axial bond length is about an order of magnitude less than the precision; the X-ray value of 2.168(5) Å should be compared with the neutron value of 2.109(1) Å. This needs to be borne in mind when considering the bond lengths derived from X-ray powder diffraction refinements on the Mn/Ni phase discussed later.

Electron microscopy

Fig. 5(a) and (b) show the electron diffraction patterns for sample **C** using the [001] and [010] zone axes respectively. Both electron diffraction patterns can be successfully indexed on the basis of the tetragonal unit cell established by powder X-ray diffraction data. The [001] zone does not show any indication of the $\sqrt{2}a \times \sqrt{2}a$ cell which would result from B-site cation ordering. The corresponding lattice images show the compound to be well ordered, the term referring to the absence of stacking faults and intergrowths in the microstructure of the crystallites.

Magnetic measurements

Fig. 6(a) and (b) show the variation of the field cooled (FC) and zero field cooled (ZFC) molar magnetisation with temperature for samples **B** and **C**. Above 190 K both samples obey the Curie–Weiss law, indicating localised electron behaviour. The corresponding values of the Curie constant (C), Weiss

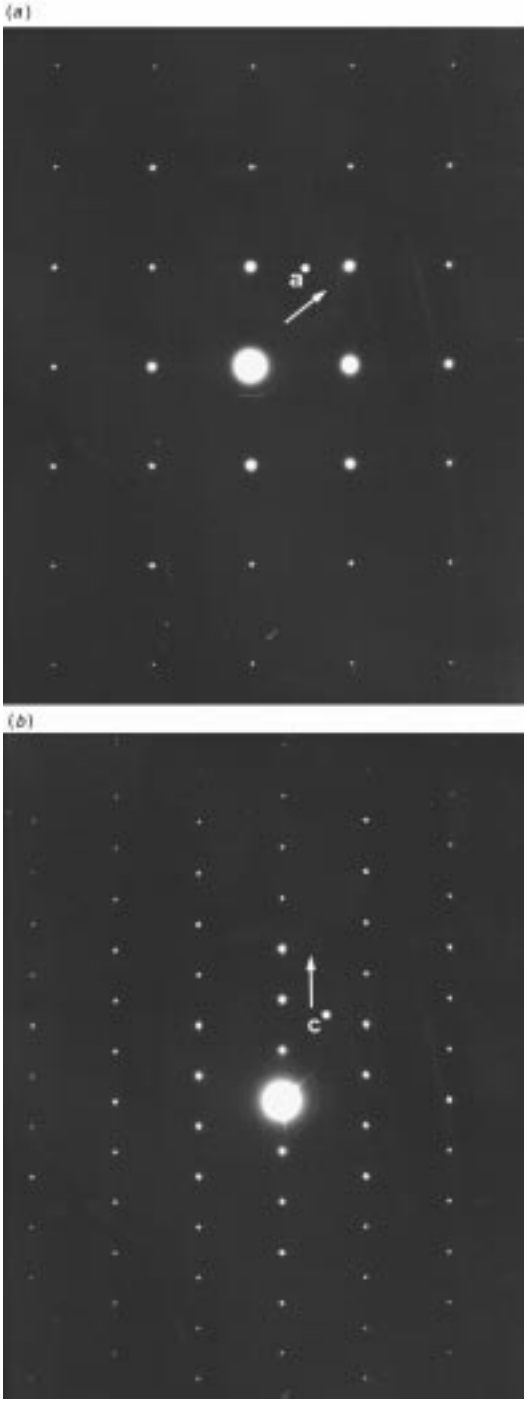

Fig. 5 (a) [001] zone axis electron diffraction pattern and (b) [010] zone axis electron diffraction patterns for $LaSrMn_{0.5}Ni_{0.5}O_4$ (sample **C**) at 293 K

constant (θ) and effective magnetic moment (μ_{obs}) are given in Table 4. Measurement of linear $M(H)$ isotherms at 298 K indicated that both compounds are conventional paramagnets at room temperature.

Both samples show divergence between the FC and ZFC magnetisations below 80 K (the divergence for sample **B** being three times larger than for **C**) and a local maximum in the magnetisation in the region $60 \leqslant T/K \leqslant 100$. The inset of Fig. 6(b) shows the maximum is at a higher temperature for the annealed sample **C** ($88 \leqslant T_{max}/K \leqslant 93$) than for **B** ($75 \leqslant T_{max}/K \leqslant 80$). In neither sample is there the pronounced global maximum in $M(T)$ found at the Néel temperature of 120 K for $LaSrMnO_4$.[30]

To investigate the irreversible behaviour further, 3 T field cooled magnetisation isotherms were measured on sample **B**

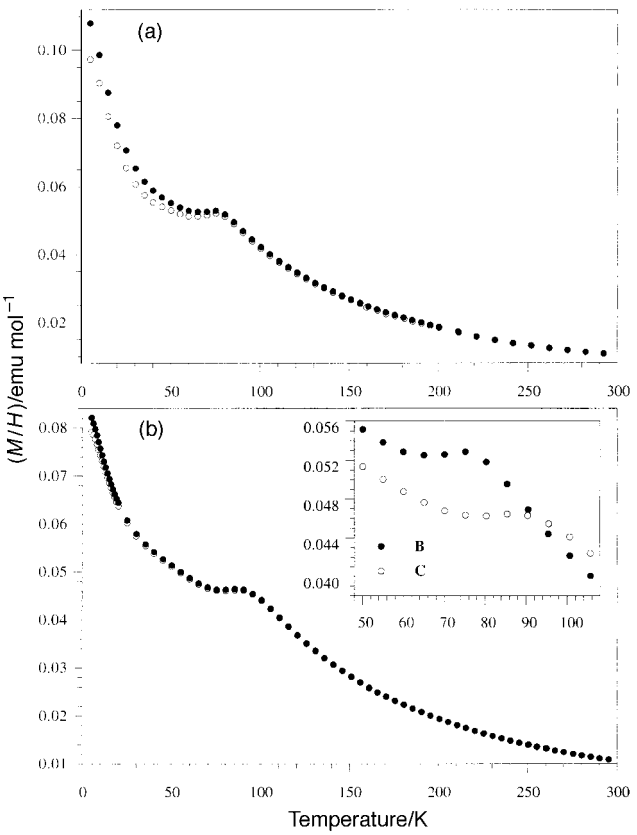

Fig. 6 Molar magnetisation as a function of temperature in a 0.01 T field for $LaSrMn_{0.5}Ni_{0.5}O_4$. (a) sample **B** and (b) sample **C**. ZFC and FC data are shown as open and filled circles respectively. The inset in (b) shows FC magnetisation data for samples **B** and **C** in the region of the local maximum.

Table 4 Curie–Weiss parameters for $LaSrMn_{0.5}Ni_{0.5}O_4$. The temperature ranges for the Curie–Weiss fits are given in brackets.

	θ/K	μ_{obs}/μ_B
sample **B** (180→300 K)	68(2)	4.40(2)
sample **C** (190→300 K)	75(1)	4.41(1)

at 200 K, 75 K and 5 K [Fig. 7(b)]. The linear $M(H)$ measurement shows the conventional paramagnetism found at room temperature is maintained at 200 K, consistent with the absence of any FC/ZFC hysteresis at this point and also confirming the absence of any $n=\infty$ contaminant. $M(H)$ becomes non-linear at 75 K, consistent with the hysteresis developing below $T(\chi_{max})$, with significant hysteresis developing at 5 K. An enlargement of a further $M(H)$ loop collected at 5 K after cooling in a field of 0.2 T is shown in Fig. 6(b). The pronounced displacement of this loop from the origin indicates that the divergence between FC/ZFC below $T(\chi_{max})$ arises not due to weak ferromagnetism associated with the ordered canting of antiferromagnetic spins, but because of the onset of spin glass-like freezing of regions of spins within the sample.

Discussion

Pure $LaSrMn_{0.5}Ni_{0.5}O_{4+\delta}$ cannot be prepared in either air or pure oxygen, due to formation of an $n=\infty$ perovskite phase, which is thermodynamically favoured in these oxidising atmospheres. Synthesis under argon is required for the preparation of single phase samples. Iodometric analysis of the oxygen content of these compounds (Table 2) shows that they are both stoichiometric within error, the annealing of sample **B** at 1300 °C in Ar to produce **C** not resulting in any detectable change in the oxygen content.

The results of thermogravimetric analyses show that complete reduction to nickel metal and manganese monoxide does not occur, even when the samples are heated to 950 °C under pure H_2 for several hours. This is a strong contrast with the behaviour of $LaSrNiO_4$ itself, which decomposes to La_2O_3, SrO and Ni under these conditions in about 30 min. However, several gradual steps in the reduction process are visible. Inspection of the reduction products by powder X-ray diffraction reveals that the K_2NiF_4 structure is not fully maintained and that the samples have partially decomposed into a mixture of Ni metal and binary oxides, suggesting that the failure to achieve complete reduction is kinetic. These results provide an interesting comparision with $LaSrCr_{0.5}Ni_{0.5}O_4$: in the Mn case, the reduction of the K_2NiF_4 structure is also considerably slowed compared to pure $LaSrNiO_4$, but, unlike Cr^{III}, Mn^{III} co-substitution is insufficient to kinetically stabilise Ni^{I} within the K_2NiF_4 structure. This is because there are stable oxides of manganese in oxidation states lower than +III which allow an easier reduction pathway for the solid when compared with the Cr^{III} case where the only possibility is reduction directly to the metal. This gives the partly reduced K_2NiF_4 phase $La_2Sr_2CrNiO_7$ considerable kinetic stability to further reduction. A comparison of the lattice parameters of the residual K_2NiF_4 phase found after the extended high temperature reduction with $LaSrMnO_4$ ($a=3.804$ Å, $c=13.10$ Å)[31] are consistent with this phase being manganese-rich.

We now consider the structural and magnetic properties in contrast with the behaviour of the $n=\infty$ $LaMn_xNi_{1-x}O_3$ perovskites. The conflicting observations and conclusions reported in the literature appear to indicate that the position of the equilibrium represented in eqn. (1) below depends upon the manganese concentration, synthesis temperature and degree of atomic ordering.

$$Ni^{II}+Mn^{IV}=Ni^{III}(LS)+Mn^{III} \quad (1)$$

Problems associated with the production of monophasic samples of $LaMn_xNi_{1-x}O_3$ with $0<x<0.5$, high temperature synthesis resulting in the formation of biphasic samples, have led to difficulties in the interpretation of the physical properties of these compounds.[18,24,25,32] Sonobe *et al.*[18] and Asai *et al.*[25] have reported ^{55}Mn NMR data that support a predominance of Mn^{IV} and Ni^{II}, although in both studies evidence for some ambiguity in this description was found. In support of such an assignment Blasse[16] reported high temperature paramagnetic susceptibility data indicating that the preferred valences at high temperature appear to be Mn^{IV} and Ni^{II}, consistent with evidence presented for at least partial ordering of the two cations. A weak {111} reflection from a doubled unit cell, characteristic of partial ordering between the Mg^{II} and Mn^{IV} ions, was observed in the powder X-ray diffraction pattern of $LaMg_{0.5}Mn_{0.5}O_3$.[16] By analogy similar cation ordering of the Ni^{II} and Mn^{IV} ions in $LaMn_{0.5}Ni_{0.5}O_3$ was proposed. The absence of such a reflection in the diffraction data collected for the latter compound and those containing Co^{II}, and Cu^{II} rather than Mg^{II}, was attributed to the reduction in contrast between the scattering powers of the ordered ions. In opposition to this assignment of valences, Vasanthacharya *et al.*[24] used X-ray absorption and photoelectron spectroscopy to establish that in their disordered samples of $LaMn_xNi_{1-x}O_3$ with $x=0.1$, 0.2 and 0.5, synthesised *via* a low temperature precursor route, Mn^{III} and Ni^{III} cations predominate at room temperature. The saturation magnetisation of the ferromagnet shows that Ni^{III} was present in its low-spin state. In addition, experimental values of the effective magnetic moments of $LaMn_xNi_{1-x}O_3$ samples with $x=0.1$, 0.2 and 0.5, are consistent with those calculated for xMn^{III} and low-spin $(1-x)Ni^{III}$.[24] These conflicting reports, and discrepancies between the Curie temperatures obtained for samples produced by different work-

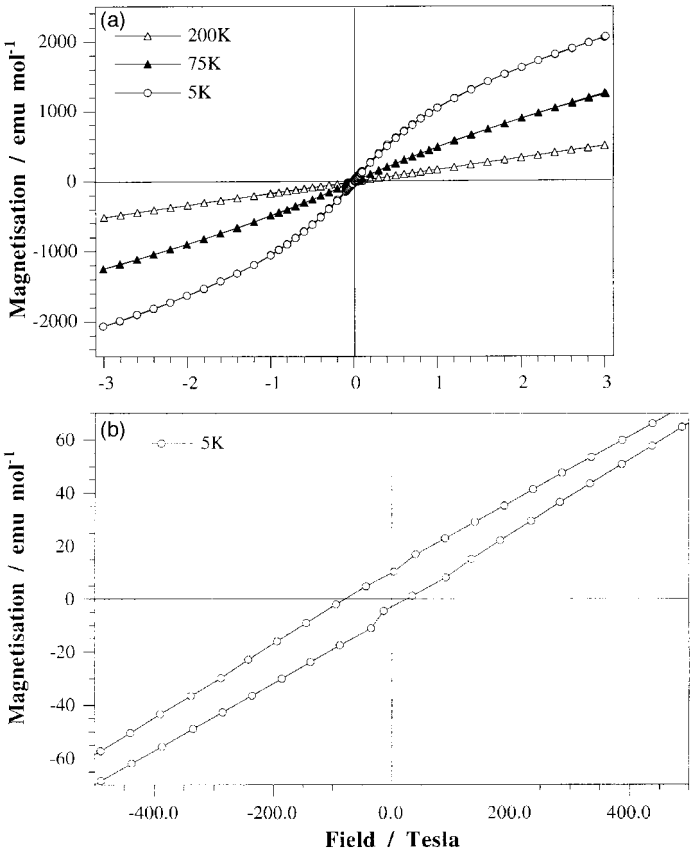

Fig. 7 Magnetisation isotherms for sample **B**. (a) Field cooled (3 T) magnetisation hysteresis loops at 200 K, 75 K and 5 K and (b) enlargement of a field cooled (0.2 T) magnetisation hysteresis loop at 5 K.

ers, indicate that the magnetic properties and relative stabilities of the possible valence states are sensitive to the degree of cation ordering, in turn dependent upon the cation oxidation states.

Two-dimensional $LaSrMn_{0.5}Ni_{0.5}O_4$ appears to be quite different from the $n=\infty$ phases. When the effective magnetic moments from fitting the high temperature susceptibility data of both samples **B** and **C** to the Curie–Weiss law, 4.40 and 4.41 μ_B respectively, are compared with those calculated on the basis of the combined non-interacting spin-only moments for equimolar mixtures of Mn^{III} and low-spin Ni^{III} (3.67 μ_B), Mn^{III} and high-spin Ni^{III} (4.42 μ_B) and Mn^{IV} and Ni^{II} (3.39 μ_B), the values obtained are clearly in excellent agreement with those expected for a combination of high-spin trivalent cations. The absence of cation ordering is consistent with the cations adopting the same oxidation state. The excellent agreement between the magnetic moments for **B** and **C** indicates that the oxidation state distribution, as well as the mean oxidation state given by iodometry, is not affected by annealing. The Curie–Weiss fits to the magnetic data above 180 K clearly indicate that, while the oxidation state distribution found by Vasanthcharya *et al.* is appropriate, it is Ni^{III} in the high spin state which coexists with Mn^{III}. The quality of the Curie–Weiss fits combined with the $M(H)$ linearity and absence of hysteresis at both 200 K and 300 K indicate that the spin–spin coupling and resultant irreversibility found at lower temperatures does not influence the magnetic behaviour in the temperature regime where the magnetic data is used to determine oxidation and spin state. The Curie law moments can therefore be considered to be reliable. Rao *et al.* have previously reported high field high temperature magnetic studies on a sample of $LaSrMn_{0.5}Ni_{0.5}O_4$, prepared by a ceramic method at 1200°C in air, although no structural data were presented.[10] Fitting the data to the Curie–Weiss law for $T<500$ K, they obtained an effective magnetic moment of 6.03 μ_B with a Weiss constant of +190 K. Clearly these values are at odds with those obtained here. In both cases the considerable positive values of θ are suggestive of significant ferromagnetic correlations within the MO_2 planes. The differences between the two sets of data presumably arise from the different synthesis conditions employed.

This change of spin state at Ni^{III} on substitution of Mn^{III} for Cr^{III} is at first sight surprising $LaSrCr_{0.5}Ni_{0.5}O_4$ shows Curie–Weiss behaviour from 10 K above its spin-glass freezing temperature of 16 K to 300 K with an observed Curie law moment of 2.91 μ_B compared with the low-spin Ni^{III}/Cr^{III} theoretical value of 3.00 μ_B.[14] In order to assess the validity of the oxidation state assignment from magnetic data, detailed consideration of the structures of the two K_2NiF_4 phases is required. The powder X-ray diffraction studies on $LaSrMn_{0.5}Ni_{0.5}O_4$ samples **B** and **C** show the compounds adopt an undistorted tetragonal K_2NiF_4 structure. There is no evidence of supercell reflections indicative of cation ordering in the diffraction patterns for either sample, although since the difference between the X-ray scattering powers of Mn and Ni is very small it would be surprising to see such weak features using a laboratory diffractometer. High resolution transmission electron microscopy studies on sample **C** enabled investigation of the microstructure of the material. The electron diffraction patterns and lattice images obtained indicate that the sample consists of well ordered crystallites each with the tetragonal K_2NiF_4 structure established by powder X-ray diffraction. There is no indication of any supercell reflections, showing that the transition metal cations in the sample are randomly distributed and that there is no tilting of the BO_6 octahedra. This in turn supports the magnetic evidence that the manganese and nickel are present as trivalent ions rather than Mn^{IV} and Ni^{II}, since as such there will be no electrostatic forces to induce ordering on the B cation sublattice. In general cation ordering in the perovskite layers of the K_2NiF_4 structure is favoured

by size and charge differences. The small difference between the ionic radii of six coordinate Mn^{III} (0.645 Å) and Ni^{III}, whether high (0.60 Å) or low-spin (0.56 Å), is alone unlikely to be sufficient to cause such ordering.[33–35] This view is supported by the observation of supercell reflections attributed to 1:1 B cation ordering for the low-spin Ni^{III} phases (A, La)$_2$M′$_{0.5}$Ni$_{0.5}$O$_4$ (A = Ca, Sr, Ba; M′ = Mg, Zn), but not for LnSrM′$_{0.5}$Ni$_{0.5}$O$_4$ (M′ = Al, Ga; Ln = La, Sm, Nd), indicating that the same charge and small size difference between the M′ and Ni^{III} ions in the latter cases cannot induce ordering.[11]

In order to assess this combination of transition metal valence and spin states, it is useful to compare the distortion of the MO_6 octahedra observed for the $LaSrMn_{0.5}Ni_{0.5}O_4$ samples with that refined for the analogous chromium compounds from neutron powder diffraction (Table 5). The phase purity of the Nd-substituted phase, and the similarity of the refined parameters (including the anisotropic displacement ellipsoids), reinforces the conclusions drawn for $LaSrCr_{0.5}Ni_{0.5}O_4$. In making this comparison, the enhanced precision of the B—O bond lengths derived from neutron powder diffraction data must be borne in mind. The values of both c/a and r[B—O(1)]/r[B—O(2)] are slightly larger than found for the Jahn–Teller Mn^{III}/non-Jahn–Teller Mn^{IV} phases $Ln_{0.5}Sr_{1.5}MnO_4$ {c/a = 3.218 (3.228), r[B—O(1)]/r[B—O(2)] = 1.04 (1.05) for Ln = La(Nd)},[5,36] indicating the presence of significant static Jahn–Teller distortion. Both the Cr/Ni phases have very similar distortions of the BO_6 octahedra, indicating a negligible effect of changes at the A site on the B site Jahn–Teller distortion, despite a significant change in the c/a ratio. This indicates, in contrast to $Sr_{1.5}Ln_{0.5}MnO_4$,[5] that lanthanide electronegativity is not important in enhancing the Jahn–Teller distortion at low-spin Ni^{III}, because, unlike the Mn case, the e_g electrons are localised in both cases in the two Cr/Ni phases studied here. The insensitivity of the BO_6 distortion to A cation size and electronegativity extends to the two samples of $LaSrMn_{0.5}Ni_{0.5}O_4$ studied here. As the octahedral distortions in the Mn/Ni samples are also similar to each other, the significant evolution in c/a on annealing can also be associated with bond length changes at the A site. From the larger value of the ratio of the axial and equatorial metal–oxygen bond lengths and c/a for the Cr/Ni compounds, it is clear that the extent of the Jahn–Teller distortion in both $LaSrCr_{0.5}Ni_{0.5}O_4$ and $La_{0.9}Nd_{0.1}SrCr_{0.5}Ni_{0.5}O_4$ is greater than that in $LaSrMn_{0.5}Ni_{0.5}O_4$. If the Ni^{III} spin state were the same in both systems, the distortion of the BO_6 octahedra, and hence c/a, would be expected to increase upon replacement of Cr^{III} by Mn^{III}, which is itself Jahn–Teller unstable. The bond length comparison is less strong on its own as the Mn/Ni—O values are only derived from X-ray powder data, although reinforced by the comparison with the neutron-derived $Ln_{0.5}Sr_{1.5}MnO_4$ values. A close analogy is available from the detailed study of the influence of Mn^{III} concentration on the structure of $NdSrGa_{1-x}Mn_xO_4$, where the c/a ratio increases sharply with x.[37] Therefore the reduced distortion in $LaSrMn_{0.5}Ni_{0.5}O_4$ compared with the analogous Cr compound is consistent with the Ni^{III} ions in the mixed Mn/Ni system no longer being Jahn–Teller active, and thus high-spin. The structural data is thus in agreement with the effective magnetic moments obtained from Curie–Weiss fits.

The change in electronic configuration of the nickel between the two systems can be rationalised in terms of the transition metal ionic radii and electronegativity. The increased electronegativity of Mn^{III} over Cr^{III} will produce greater competition for bonding with oxide, weakening covalency with Ni^{III} and thus favouring the high-spin state. Similar arguments have been developed by Demazeau and co-workers in studying the high spin–low spin transition in Co^{III} oxides.[38] In ionic model terms, high spin (d^4) Mn^{III} (0.645 Å) is significantly larger than (d^3) Cr^{III} (0.615 Å), and so replacement of chromium by manganese will favour high-spin (0.60 Å) as compared to low-spin (0.56 Å) d^7 Ni^{III} by lengthening the average B—O bond length and hence reducing the crystal field.[33–35] This view is qualitatively consistent with the observed increase in the a lattice parameter and B—O(2) equatorial bond in the Mn samples. An interesting quantitative argument based solely on the lattice parameters, which can be confidently related to the mean B—O bond lengths because the electron and neutron diffraction data show that there are no octahedral tilts, can be constructed by noting that the two K_2NiF_4 phases $NdSrCrO_4$ and $NdSrMnO_4$[39] differ in equatorial B—O bond length by 0.033 Å. This leads to a predicted increase in a from $LaSrMn_{0.5}Ni_{0.5}O_4$ to $LaSrCr_{0.5}Ni_{0.5}O_4$ of 0.033 Å if the spin state and thus ionic radius of Ni^{III} remains unchanged. The observed decrease in a of 0.011 Å can be considered to result from this combined change in radius from Mn^{III} to Cr^{III} plus the change in effective radius of Ni^{III} between the two compounds which may be computed as −0.044 Å. This Ni^{III} radius change is exactly equal to the difference in Shannon–Prewitt radii of low-spin and high-spin Ni^{III}. While the almost exact agreement is clearly fortuitous, both the evolution of the lattice parameters (which are accurately determined by X-rays) and the B—O bond length from the Cr to the Mn-substituted phases are consistent with the change in Ni^{III} spin state shown by the magnetic data.

Substitution of localised low-spin Ni^{III} into the antiferromagnet $LaSrCrO_4$ produces both disorder and frustration leading to canonical spin-glass behaviour with a freezing temperature T_F beneath which the magnetisation no longer increases on cooling. The data presented here also indicate that the introduction of high spin Ni^{III} into $LaSrMnO_4$ suppresses the long-range antiferromagnetic ordering observed at 120 K; the Néel point is replaced by a local anomaly in M between 80 and 90 K below which M continues to increase on cooling and hysteresis between field-cooled (FC) and zero-field cooled (ZFC) data is observed. This suggests that the antiferromagnetic ordering is suppressed, although low temperature neutron powder diffraction would be required to confirm this. The observed hysteresis and, importantly, the sensitivity of the local maximum to annealing discussed later, indicate that any antiferromagnetic order would involve a considerably reduced B-site staggered moment. The FC/ZFC hysteresis and displaced field cooled hysteresis loop at low temperature indicate that the dynamics of regions of spins in the sample are slowing on cooling below the local maximum, with the frozen regions having unidirectional anisotropy consistent with spin-glass

Table 5 Comparison of structural data for $LaSrMn_{0.5}Ni_{0.5}O_4$ (samples **B** and **C**), $La_{0.9}Nd_{0.1}SrCr_{0.5}Ni_{0.5}O_4$ and $LaSrCr_{0.5}Ni_{0.5}O_4$. Δ(M—O) is the difference between the axial and equatorial bond lengths of the B site, while Σ(M—O) is their sum

	$LaSrMn_{0.5}Ni_{0.5}O_4$			
sample	**B**	**C**	$La_{0.9}Nd_{0.1}SrCr_{0.5}Ni_{0.5}O_4$	$LaSrCr_{0.5}Ni_{0.5}O_4$
c/a	3.2728(1)	3.28086(8)	3.30121(5)	3.30221(2)
M—O(1) axial/Å × 2	2.05(1)	2.060(8)	2.1036(4)	2.109(1)
M—O(2) equatorial/Å × 4	1.91798(6)	1.91943(2)	1.91144(1)	1.91378(1)
M—O(1)/M—O(2)	1.069(5)	1.073(4)	1.1005(2)	1.1020(5)
Δ(M—O)/Σ(M—O)	0.033(2)	0.035(1)	0.04786(9)	0.0485(2)

character and producing the displaced hysteresis loop. The $LaSrMn_{0.5}Ni_{0.5}O_{4+\delta}$ samples do not however display canonical spin-glass magnetic behaviour at low temperature; rather than a well defined freezing temperature, the irreversible magnetism appears related to intrinsic inhomogeneities. The continued increase in M on cooling below the local maximum to 5 K indicates that all the spins in the sample do not freeze or order antiferromagnetically, while the hysteresis indicates some cooperative slowing of the spin dynamics in at least regions of the sample. An estimate of the fraction of spins frozen may be given by noting that M doubles from 240 K to 120 K in agreement with Curie predictions but that there is only a 30% increase from 120 K to 60 K, suggesting that the process producing the local maximum involves the ordering/freezing of 2/3 of the spins. For sample **B**, divergence between the FC and ZFC magnetisations begins at 75 K, coincident with the local maximum in $M(T)$. FC $M(H)$ measurements at 5 K produce a hysteresis loop which is displaced from the origin. $M(H)$ measurements at the temperature of the maximum, 75 K, do not show such hysteresis despite being non-linear (sigmoidal), suggesting that small clusters of superparamagnetic spins form below 180 K when the Curie–Weiss law breaks down.

Having established the Mn and Ni spin and oxidation states and the existence of inhomogeneous irreversible magnetism, it is necessary to consider the possible outcome of 180° superexchange between Mn^{III} and high-spin Ni^{III}. The electron diffraction studies for sample **C**, combined with the neutron powder diffraction evidence, show there is no tilting of the MO_6 octahedra and therefore the B—O—B bond angles are 180°, simplifying the discussion considerably.[40] The high temperature Curie behaviour shows that, similar to the effect of Cr^{III} substitution, the introduction of Mn^{III} localises the itinerant electrons in $LaSrNiO_4$. The high-spin Ni^{III} introduces competing superexchange interactions, but in a more complex manner than the effect of Cr^{III}–Ni^{III} coupling on transforming antiferromagnetic $LaSrCrO_4$ to spin-glass $LaSrCr_{0.5}Ni_{0.5}O_4$. The positive Weiss constant compared to the small negative values obtained in the $LaSrCr_xNi_{1-x}O_{4+\delta}$ series, is consistent with considerably enhanced ferromagnetic interactions in the Mn/Ni system. The Ni^{III}—O—Ni^{III} interactions will be antiferromagnetic (AF) when the Ni^{III} is high-spin, but are insufficient to produce antiferromagnetic long-range order in isolation as the system is below the 58% site percolation threshold for a two-dimensional square array. The sign of Mn^{III}—O—Mn^{III} superexchange will depend critically on the presence of a Jahn–Teller distortion and any local co-operative orbital ordering, both ferromagnetic (F) and AF ordering being possible. This contrasts with Cr^{III}—O—Cr^{III} 180° superexchange in the spin-glass $LaSrCr_{0.5}Ni_{0.5}O_4$ which can only be AF. Coupling involving overlap between the half-filled and empty orbitals of two Jahn–Teller distorted cations will be F, while that between two half-filled orbitals will be AF. In $LaSrMnO_4$ itself, ordering of the e_g^1 electron into the z^2 orbital in a ferroelastic manner produces the enhanced c/a and accounts for the observed antiferromagnetic coupling of all four near neighbours in the xy plane found by neutron diffraction, with the moments aligned along the interlayer direction.[41] Mn^{III}–Mn^{III} superexchange coupling when the crystalline environment does not produce a static distortion is F *via* correlation of the superexchange charge transfer by a dynamic Jahn–Teller mechanism.[17,24] The Mn^{III}–Mn^{III} coupling is thus extremely sensitive to the precise splitting of the degenerate e_g orbitals: comparison of the bond lengths with the pure Mn^{III} solid suggests that the Jahn–Teller splitting is reduced, although a direct local measurement of the Mn—O coordination would be preferable, while the orbital ordering characteristic of pronounced ferroelastic Jahn–Teller elongation will give AF coupling as in $LaSrMnO_4$. The Mn–Mn coupling may thus be either F or AF depending on the details of the local environment of the manganese. The sign of superexchange coupling between high spin Ni^{III} and Mn^{III} with the e_g electron ordered in the z^2 orbital depends on the relative strength of couplings between z^2 and x^2-y^2 orbitals: it will be F if dominated by the half-filled—empty x^2-y^2—x^2-y^2 hopping, and presumably sensitive to local distortions, thus presenting both a source of annealing dependence and contrast with the Cr/Ni phases. The key difference here from both the $LaSrCr_{1-x}Ni_xO_4$ ($B=Cr^{III}$, $B'=Ni^{III(LS)}$) and $La_{1-x}Sr_{1+x}MnO_4$ ($0.2\leqslant x\leqslant 0.6$; $B=Mn^{III}$, $B'=Mn^{IV}$) phases (which display straightforward low-temperature spin glass-like freezing[14,30]) is that in the Mn/Ni case both B site cations carry e_g electrons, making their exchange interactions sensitive to the nature of local Jahn–Teller distortions, while the B–B′ interactions in the pure spin glass phases are unambiguously ferromagnetic (Mn^{III}/Mn^{IV} and $Cr^{III}/Ni^{III(LS)}$).

Annealing sample **B** to produce **C** reduces the extent of the FC/ZFC divergence while simultaneously increasing the temperature of the local maximum, but has no effect upon the observed effective magnetic moment at high temperatures ($190\leqslant T/K\leqslant 300$). This suggests that the B site cation distribution is inhomogeneous but not ordered over a sufficient distance to produce Bragg peaks even in electron diffraction, and that the extent of inhomogeneity is reduced on annealing. In the case of the canonical RKKY spin glass CuMn, annealing increases the spin freezing temperature by removing the smearing of the freezing which arises from dopant inhomogeneity and clustering.[42] Consistent with this, analysis of the X-ray data after the high-temperature anneal indicates that the scattering domain size has increased substantially from 650 Å to over 2000 Å (calculated using the Scherrer formula; the pattern does not display anisotropic broadening) and the strain broadening (measured by the $\tan\theta$ dependent part of the Lorentzian component of the peakshape) has decreased from 0.29% to 0.05%, consistent with a reduction in the extent of chemical short-range ordering. The subtle influence of annealing on the low-field low temperature magnetism plus the slight change in Weiss constant can thus be assigned to changes in the local disorder of Mn and Ni, altering the lifting of the e_g degeneracy at Mn^{III} and thus the distribution of superexchange couplings involving manganese.

The contrasts with the three-dimensional perovskite $LaMn_{0.5}Ni_{0.5}O_3$, which behaves like a classical ferromagnet, are that in the perovskite the e_g degeneracy at Mn is not lifted by static distortions and the Ni^{III} is low spin. The spin state change can be associated with a considerably shorter mean bond length in the perovskite of 1.938 Å[24] (computed from the pseudocubic lattice parameter and compared with 1.964 Å in the $n=1$ phase), possibly produced by tolerance factor considerations and the enhanced size of Sr^{2+} (1.44 Å) over La^{3+} (1.30 Å). These two features make the superexchange interactions between all the possible pairs of cations ferromagnetic, resulting in three-dimensional ferromagnetic behaviour. In the present two-dimensional system, the crystal field partly lifts the e_g degeneracy at Mn, producing predominantly ferromagnetic interactions but no long-range order because the absence of site percolation in two dimensions is combined with the competing antiferromagnetism produced by the introduction of high-spin Ni^{III}. Regions of spins then freeze below a temperature close to the ferromagnetic Weiss temperature found from the high temperature susceptibility, suggesting that the local maximum is related to the interactions probed at high temperature. Spin-state changes induced by changing n in Ruddlesden–Popper phases have recently been identified in the $Sr_{n+1}Ru_nO_{3n+1}$ series, with $n=1$ Sr_2RuO_4 having high-spin Ru^{IV}[43] in contrast to the $n=2$ and $n=\infty$ phases.[44]

In conclusion, 50% substitution of Mn^{III} for Ni^{III} in $LaSrNiO_4$ produces high-spin rather than low-spin Ni^{III}, in contrast to Cr^{III} substitution. This is confirmed by both structural and magnetic measurements. The substitution produces

neither canonical spin glass behaviour as in the $LaSrCr_xNi_{1-x}O_{4+\delta}$ series, nor the ferromagnetism observed for the analogous 3D perovskite series, $LaMn_xNi_{1-x}O_3$. The maxima observed in the magnetisation at *ca.* 75 K and divergence between the FC and ZFC magnetisation below this temperature result from a freezing/cluster-blocking transition to a glassy state, indicated by the displaced FC hysteresis loop obtained at 5 K. The complexity of the magnetism suggests the influence of the size of local Jahn–Teller distortions introduced by the substitution of Mn^{III} on orbital ordering and superexchange must be more subtle than is the case with the isotropic Cr^{III} cation. This influence of co-substituent size on B cation spin state is an added complication in interpreting the behaviour of Ruddlesden–Popper phases with B site substitution.

We thank the donors of the Petroleum Research Fund, administrated by the American Chemical Society, and the UK EPSRC for support of this work. Dr J. Sloan (Inorganic Chemistry Laboratory and Department of Materials, University of Oxford) kindly carried out the electron diffraction study on sample **C**.

References

1 C. H. Chen, S.-W. Cheong and A. S. Cooper, *Phys. Rev. Lett*., 1993, **71**, 2461.
2 S.-W. Cheong, H. Y. Hwang, C. H. Chen, B. Batlogg, L. W. Rupp and S. A. Carter, *Phys. Rev. B, Rapid Commun*., 1994, **49**, 7088.
3 P. G. Radaelli, D. E. Cox, M. Marezio and S. W. Cheong, *Phys. Rev. B*, 1997, **55**, 3015.
4 B. J. Sternlieb, J. P. Hill, U. C. Wildgruber, G. M. Luke, B. Nachumi, Y. Moritomo and Y. Tokura, *Phys. Rev. Lett*., 1996, **76**, 2169.
5 Y. Moritomo, A. Nakamura, S. Mori, N. Yamamoto, K. Ohoyama and M. Ohashi, *Phys. Rev. B*, 1997, **56**, 14879.
6 R. Gundakaram, A. Arulraj, P. V. Vanitha, C. N. R. Rao, N. Gayathri, A. K. Raychaudhuri and A. K. Cheetham, *J. Solid State Chem*., 1996, **127**, 354.
7 I. O. Troyanchuk, N. V. Samsonenko, N. V. Kasper, H. Szymczak and A. Nabialek, *J. Phys. Condens. Matter*, 1997, **9**, 8287.
8 T. C. Gibb and R. J. Whitehead, *J. Mater. Chem*., 1993, **3**, 591.
9 A. Skowron, A. Petric, H. Moudallal, A. J. Jacobson and C. A. Mims, *Mater. Res. Bull*., 1997, **32**, 327.
10 C. N. R. Rao, P. Ganguly, K. K. Singh and R. A. Mohan Ram, *J. Solid State Chem*., 1988, **72**, 14.
11 S. H. Byeon, G. Demazeau and J. H. Choy, *Jpn. J. Appl. Phys*., 1995, **34**, 6156.
12 Z. L. Ming, G. Demazeau, M. Pouchard, J. M. Dance and P. Hagenmuller, *J. Solid State Chem*., 1989, **78**, 46.
13 R. A. M. Ram, K. K. Singh, W. Madhusudan, P. Ganguly and C. N. R. Rao, *Mater. Res. Bull*., 1983, **18**, 703.
14 J. E. Millburn and M. J. Rosseinsky, *Chem. Mater*., 1997, **9**, 511.
15 T. Strangfeld, K. Westerholt and H. Bach, *Physica C*, 1991, **183**, 1.
16 G. Blasse, *J. Phys. Chem. Solids*, 1965, **26**, 1969.
17 J. B. Goodenough, A. Wold, R. J. Arnott and N. Menyuk, *Phys. Rev*., 1961, **124**, 373.
18 M. Sonobe and A. Kichizo, *J. Phys. Soc. Jpn*, 1992, **61**, 4193.
19 I. O. Troyanchuk, H. Szymczak, N. V. Samsonenko and A. Nabialek, *Phys. Status Solidi*, 1996, **157**, 167.
20 I. O. Troyanchuk, N. V. Samsonenko, E. F. Shapovalova, H. Szymczak and A. Nabialek, *Mater. Res. Bull*., 1997, **32**, 67.
21 N. Y. Vasanthacharya, K. K. Singh and P. Ganguly, *Rev. Chim. Miner*., 1981, **18**, 333.
22 P. Ganguly, N. Y. Vasanthacharya, C. N. R. Rao and P. P. Edwards, *J. Solid State Chem*., 1984, **54**, 400.
23 D. D. Sarma, O. Rader, T. Kachel, A. Chainani, M. Mathew, K. Holldack, W. Gudat and W. Eberhardt, *Phys. Rev. B*, 1994, **49**, 14238.
24 N. Y. Vasanthacharya, P. Ganguly, J. B. Goodenough and C. N. R. Rao, *J. Phys. C: Solid State Phys*., 1984, **17**, 2745.
25 K. Asai, H. Sekizawa and S. Iida, *J. Phys. Soc. Jpn*., 1979, **47**, 1054.
26 H. M. Rietveld, *J. Appl. Crystallogr*., 1969, **2**, 65.
27 A. C. Larson and R. B. von Dreele, General Structural Analysis Systems, Los Alamos National Laboratory, 1994.
28 M. Karppinen, A. Fukuoka, L. Niinisto and H. Yamauchi, *Supercond. Sci. Technol*., 1996, **9**, 121.
29 A. I. Vogel, *A Textbook of quantitative inorganic analysis*, Longmans, London, 1961.
30 Y. Moritomo, Y. Tomioka, A. Asamitsu and Y. Tokura, *Phys. Rev. B*, 1995, **51**, 3297.
31 A. Benabad, A. Daoudi, R. Salmon and G. L. Flem, *J. Solid State Chem*., 1977, **22**, 121.
32 A. Wold and R. J. Arnott, *J. Phys. Chem. Solids*, 1959, **9**, 176.
33 R. T. Shannon and C. T. Prewitt, *Acta Crystallogr., Sect. B*, 1969, **25**, 925.
34 R. T. Shannon and C. T. Prewitt, *Acta Crystallogr., Sect. B*, 1970, **26**, 1046.
35 R. T. Shannon and C. T. Prewitt, *Acta Crystallogr., Sect. A*, 1976, **32**, 751.
36 J.-C. Bouloux, J.-L. Soubeyroux, A. Daoudi and G. L. Flem, *Mater. Res. Bull*., 1981, **16**, 855.
37 D. Reinen, U. Kesper and D. Belder, *J. Solid State Chem*., 1995, **116**, 355.
38 G. Demazeau, S. H. Byeon, P. Hagenmuller and J. H. Choy, *Z. Anorg. Allg. Chem*., 1992, **610**, 91.
39 K. Sander, U. Lehmann and H. Muller-Buschbaum, *Z. Anorg. Allg. Chem*., 1981, **480**, 153.
40 T. C. Gibb, *J. Chem. Soc., Dalton Trans*., 1984, **4**, 667.
41 S. Kawano, N. Achiwa, N. Kamegashira and M. Aoki, *J. Phys. C*, 1988, **8**, 829.
42 A. Kalk, H. Pinkvos, C. Schwink, F. N. Gygax and A. Schenck, *J. Magn. Magn. Mater*., 1991, **102**, 184.
43 H. K. Muller-Buschbaum and J. Wilkens, *Z. Anorg. Allg. Chem*., 1990, **591**, 161.
44 M. Itoh, M. Shikano and T. Shimura, *Phys. Rev. B*, 1995, **51**, 16432.

Paper 8/00585K; *Received* 21*st January*, 1998